Combined Macro-Meso Scale Modeling of Sintering. Part II, Mesoscale Simulations

Veena Tikare*, Eugene A. Olevsky# and Michael V. Braginsky*
*Sandia National Laboratories
Albuquerque, NM 87185-1411
#San Diego State University
San Diego, CA

ABSTRACT: A mesoscale, kinetic Monte Carlo model is presented to simulate microstructural evolution during sintering of 2D complex microstructures which evolves by grain growth, pore migration and densification. No assumptions about the geometry of the evolving microstructure are made. The results of these simulations are used to generate sintering stress and normalize viscous bulk modulus for use in continuum level simulation of sintering. The advantage of these simulations is that they can be used to generate more accurate parameters as very assumptions regarding geometry and transport mechanism are made. The previous companion paper used the results from the mesoscale simulations to simulate shrinkage and warpage in sintering of bilayer ceramics.

1. Introduction

Continuum theory of sintering is well developed as seen from the previous companion paper [1]. However, the exact values of the material characteristics necessary for accurate simulations such as sintering stress and the bulk viscous modulus of a porous body are not widely available for most sintered materials. Many of analytical expressions for these parameters make simplifying geometric assumptions to make the problem analytically tractable. In this paper, we present a mesoscale model that can simulate the microstructural evolution of sintering in 2D powder compacts. The details of microstructural evolution can be used to obtain more accurate solutions for sintering stress and the bulk modulus necessary for macroscale simulation of sintering.

The model used in this study is a kinetic, Monte Carlo (KMC) model that can simulate coarsening of grains by short range diffusion across grain boundaries, pore migration and pore coarsening by surface diffusion, vacancy diffusion along grain boundaries and vacancy annihilation at the grain boundaries. This model produces images of the microstructure as a function of time. This time sequence is related to real time linearly. These series of microstructural images can be used to calculate any parameters that the simulator wishes, which in our case are sintering stress and bulk viscous modulus.

1.1 Current mesoscale models. Many researchers have studied microstructural evolution during sintering starting from the late 1940's when Kuczynski [2], Kingery [3], Exner [4,] Johnson [5], Coble [6], Ashby [7] and others [8,9,10], considered sintering of idealized powder compacts consisting of 2 or 3 spherical particles of equal size sintering by varios diffusion mechanisms. These models were used primarily to predict interparticle neck size and shrinkage as functions of diffusion mechanisms, diffusion coefficients, interfacial energies, grain size and other materials properties and geometric measures. However, the main accomplishment of these early models was in understanding the driving forces, transport mechanisms and densification processes for sintering of crystalline materials. Next, sintering models consisting of repeating unit cells of the same geometry were proposed by DeHoff [11], Bouvard and McMeeking [12], Riedel and co-workers

DISCLAIMER

DISCLAIMER

Portions of this document may be illegible in electronic image products. Images are produced from the best available original document.

[13,14] and others [15,16,17]. In these models, researchers extended the two and three particle systems to idealized repeating unit cell models where each cell consists of a grain and the porosity around it. This allowed getting more detailed information about the shapes of grains and pores during both the intermediate sintering stage where the solid and porous phase are interconnected and the final sintering stage where pores become isolated. In the last 10 years, numerical simulations of sintering have been used by many to study sintering. Molecular dynamics simulations used to study the sintering of nano-particles [18,19] showed that additional mechanisms such as particle rotation may be active in nano-systems. Continuum mechanics modeling of sintering of two [20], three [21] and a row [22] of particles have given very accurate particle shapes evolution. Application of continuum thermodynamic principles by finite difference method to simulate sintering of two particles [23], a row and close-packed particle [12], and unit cells of different packing [13] have also given more accurate data about the shrinkage kinetics during sintering. A cellular model [24] was also used to study sintering by surface diffusion in a many particle system and an MC model [25] was used to simulate final-stage sintering of many grains. In addition some of these idealized geometric simulations [12,13,14] have been used to obtain the sintering stress necessary for modeling sintering at the continuum level.

All of these numerical simulations have provided insight into the sintering problem and have provided more accurate results for densification and other important parameters. However, with the exception of two [24,25], they are still far from being a true mesoscale simulation of sintering as only a few sintering particles are considered. The two mesoscale simulations are limited to viscous phase sintering [24] in amorphous materials and to final stage sintering in crystalline materials [25]. In this paper, we show that a kinetic, Monte Carlo model can be used to simulate sintering at the mesoscale consisting of hundreds of particles. These mesoscale simulations can be used to obtain much of the same information that have been obtained from most of the analytical and numerical models referenced above. However, with proper use of this KMC simulation, very few assumptions about the geometry of the particles and their evolution have to be made. Thus, more general thermodynamic (sintering stress and bulk modulus) and kinetic data (densification rate, etc.) for sintering can be obtained from the KMC simulation.

1.2 Review of Monte Carlo models. KMC models have been used extensively to simulate problems of microstructural evolution in materials. The first KMC models were used to simulate normal grain growth in single-phase materials [26,27]. It has been shown [28] that very good representation of grain structure, topology and kinetic data could be obtained from KMC simulations. Since then, KMC models have been used to study many other types of microstructural evolution including abnormal grain growth, recrystallization [29], phase transformations, Ostwald ripening [30], pore migration [31] and final-stage sintering [25] The earliest attempt to simulate sintering using KMC models was limited to final stage sintering and implemented densification by expanding the area of the simulation as densification proceeded. The criterion for densification was to reduce porosity in proportion to the mean distance between pores in the simulation. A more fundamental method for implementing the densification by annihilation of vacancies for all stages of sintering is presented in this paper. Furthermore, the vacancy creation in this simulation is integrated more closely with other microstructural evolution processes in this simulation presented here.

While KMC models are fundamentally stochastic, the results of the studies cited above are very stable and have been found to always converge to the same topological and kinetic solutions [32]. The reason for this stability and predictability is that while any given event is stochastic, when these events are integrated over space (integrated over

microstructural features such as interfaces and area of different phases) and over time (the movement of interfaces in response to the local microstructural features) they converge to the continuum thermodynamic and kinetic results. The advantage of the KMC models is that they simulate the evolution of individual features in response to the local microstructure without making the mean field assumptions that analytical model must assume in order to obtain solutions.

2. Model Description

A KMC model was used to simulate 2D microstructural evolution during isothermal sintering. The model presented here is limited to consideration of the following processes:

1. Grain growth by short range diffusion of atoms from one side of the grain boundary to the other;
2. Long range diffusion of material to pores by grain boundary diffusion and surface diffusion;
3. Vacancy annihilation at grain boundaries.

In the model, an ensemble of grain sites and pore sites is allowed to populate a square lattice. The grain sites can assume one of Q distinct, degenerate states, where the individual state is designated by the symbol q and the total number of states in the system is Q, $q_{grain} = [1, 2, \ldots Q]$. The pore sites can assume only one state, $q_{pore} = -1$. Contiguous grain sites of the same state q form a grain and contiguous pore sites form a pore. Grain boundaries exist between neighboring grain sites of different states, q, and pore-grain interfaces exist between neighboring pore and grain sites. The equation of state for these simulations is the sum of all the neighbor interaction energies in the system given by

$$E = \frac{1}{2}\sum_{i=1}^{N}\sum_{j=1}^{8}\left(1-\delta\left(q_i, q_j\right)\right) \qquad \text{eq. 1}$$

where N is the total number of sites, δ is the Kronecker delta with $\delta(q_i = q_j) = 1$ and $\delta(q_i \neq q_j) = 0$, q_i is the state of the grain or pore at site i and q_j is the state of the nearest neighbor at site j. Thus, the only energy considered in the simulation is the interfacial energy and all unlike neighbors contribute one arbitrary unit of energy to the system. As pore sites can assume only one state, $q_{pore} = -1$, there are no pore boundaries and all pores sites coalesce. In contrast, grain sites can assume many different states making grain boundaries possible. This yields a two-component, two-phase system with uniform, isotropic interfacial energies between grains and between grains and pores.

Grain growth is simulated using the method developed in previous works [26,27,28,29]. First a grain site is chosen at random from the simulation space. Then a new state q is chosen at random from the Q possible states in the system. The grain site is temporarily assigned the new state and the change in energy is evaluated using eq. 1. Next the standard Metropolis algorithm is used to perform the grain growth step based on Boltzmann statistics. A random number, R, between 0 and 1 is generated. The transition probability, P, is calculated using

$$P = \begin{cases} \exp\left(\dfrac{-\Delta E}{k_B T}\right) & for \quad \Delta E > 0 \\ 1 & for \quad \Delta E \leq 0 \end{cases} \qquad \text{eq. 2}$$

where k_B is the Boltzmann constant and T is temperature. If the $R \leq P$, then the grain growth step is accepted, if not, the original state is restored. The simulation temperature used for grain growth was $k_BT = 0$, which has been shown to simulate grain growth well [28].

Pore migration is simulated using conserved dynamics [25], so that the total number of pore sites and grain sites is the same after a pore migration step. A pore site is chosen and next a neighboring grain site is chosen. The two sites are temporarily exchanged with the grain site assuming a new state q where q results in the minimum energy. This minimum-energy, pore-grain exchange simulates pore migration by surface diffusion [33]. The change in energy for this exchange is calculated using eq. 1 and again the standard Metropolis algorithm is used to perform the pore migration step using eq. 2 to determine the transition probability. The simulation temperature used for the pore migration step was $k_BT = 0.7$. This higher temperature was necessary to simulate pore migration and is discussed in another work [34].

Densification [35] in crystalline solids occurs by vacancy annihilation at the grain boundaries. This process may be visualized as described by DeHoff [11] as vacancies being painted on the grain boundary, then an entire monolayer of the vacancies being annihilated with the center of mass of the adjacent grains moving towards that grain boundary. The rate limiting step is for vacancies to diffuse to and cover the entire grain boundary. In the MC model is a vacancy is defined as a single, isolated pore site that is not connected to any other pore sites. The algorithm used for pore annihilation is the following. A pore site is chosen. If it happens to be a vacancy, an isolated pore site, on a grain boundary, it is annihilated. The frequency of the annihilation attempts is adjusted to simulate the diffusion of vacancies to the entire grain boundary. Annihilation is simulated as follows. A straight line is drawn from the isolated pore site through the center of mass of the adjacent grain to the outside boundary of the sintering compact. Next, the isolated pore site and the outside grain site are exchanged with the grain site assuming the q state of the adjacent grain. This algorithm conserves mass globally, moves the center of mass of the adjacent grain towards the annihilation site, and annihilates a vacancy. This algorithm to simulate densification does have the artifact of moving mass from the outside boundary of the simulation to the interior. However, this artifact was found to have a negligible effect on simulation results and is discussed in another paper [36].

Time in the KMC model is measured in units of Monte Carlo step; 1MCS corresponds to N attempted changes where N is the total number of sites in the system. MC time is linearly proportional to real time. The proportionality constant of a given material can be found by comparing simulation microstructural evolution to that of the material.

4. Results

3.1 Microstructural Evolution. The algorithm described above was applied to a 2D microstructure consisting of 30% initial porosity with simulation size of 500 x 500. The starting microstructure had grains of size $d_g = 10.6$ and pores of size $d_p = 11.1$, where d is the diameter of a circle of equivalent area. The initial ratio of grain growth to pore migration to pore annihilation attempts is 10:10:1. Then the ratio changes to 10:10:n, where n is chosen to ensure the simulation of vacancy annihilation in proportion to diffusion along the length of the grain boundary. Thus, curvature driven grain growth, mass transport by grain boundary diffusion, and pore annihilation at the grain boundaries is

simulated simultaneously. The result of such simulations, microstructures at various stages during KMC simulation of sintering, are shown in figure 1.

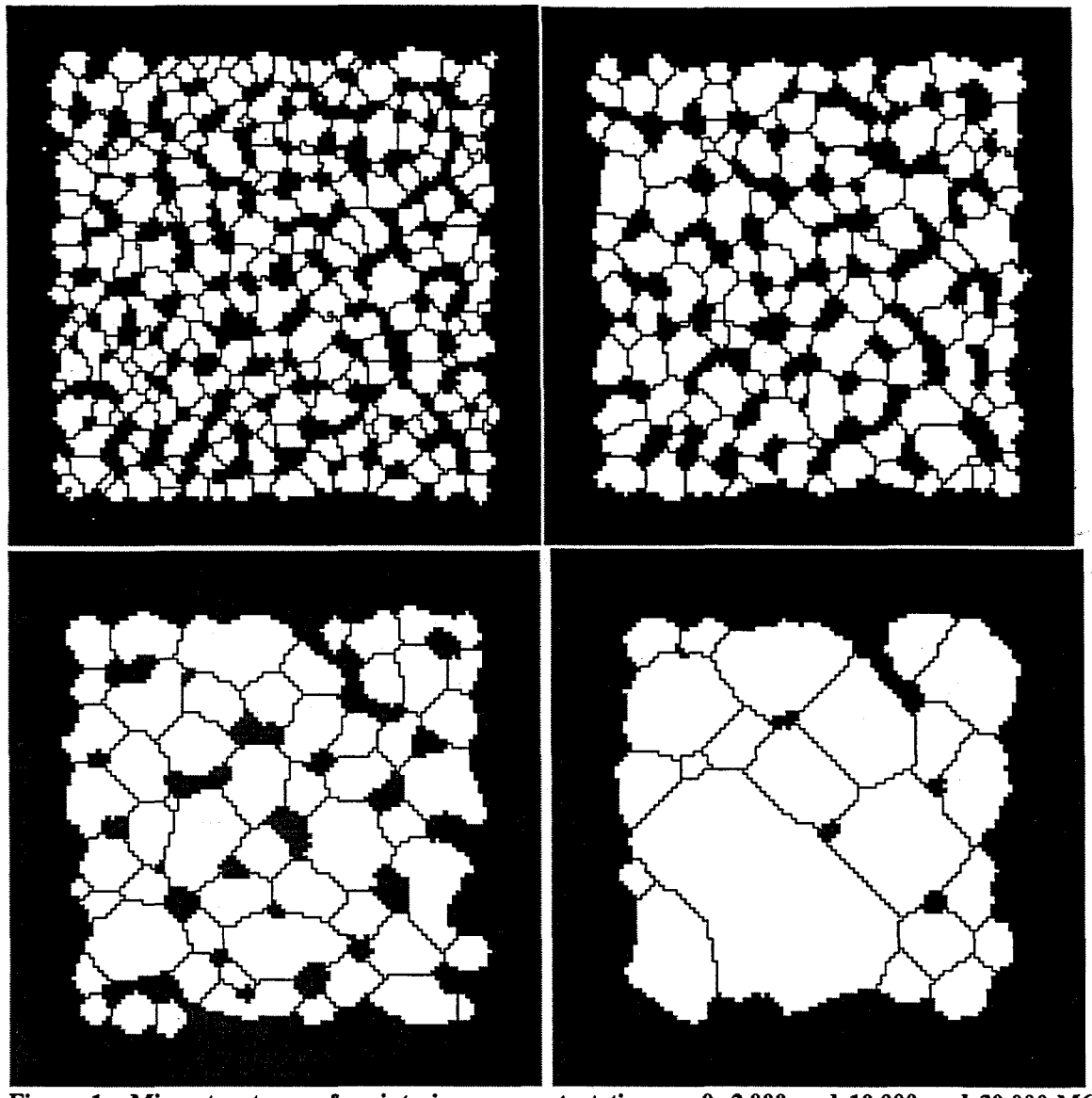

Figure 1. Microstructures of a sintering compact at times = 0, 2,000 and 10,000 and 30,000 MCS. Grains are the white features separated by black grain boundaries. Pores are drawn in grey.

The microstructures show that initially grains are very fine and many pores are interconnected, spanning several grains. As the simulation continues, grains grow, the number of pores decreases, pores become increasingly isolated and densification occurs as pores shrink and disappear. The final microstructure at time t = 100,000 MCS, shows an almost fully-dense microstructure with grains that are 2 orders of magnitude larger in area than the starting microstructure. These characteristics can be quantified as a function of time and are presented in figures 2 and 3. Figure 2 is a plot of density as a function of simulation time. Rapid densification occurs early in the simulation when both grains and pores are small and have highly curved surfaces. Rapid densification at early times is observed in the overwhelming majority of materials. Figure 3 is a plot of grain size and pore size as a function of time. Grains grew during the entire simulation. This was anticipated and is observed in most experimental systems. Pore size remained almost constant as densification progressed suggesting that pore grew by coalescence as

curves overall porosity decreased by annihilation. The microstructures shown in figure 1 are produced from a simulation of size 100 x 100. However, the data shown in figures 2 and 3 are from a simulation of size 500 x 500. The smaller simulation is shown in figure 1, so that the microstructural features may be seen more clearly.

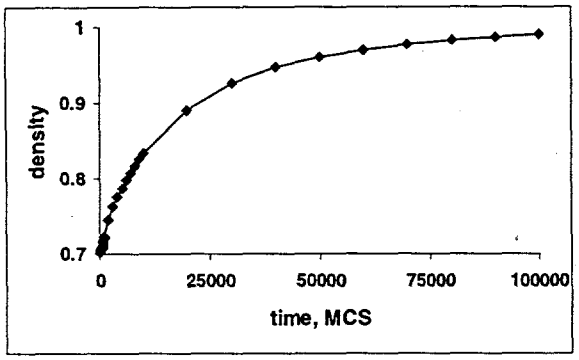

Figure 2. Densification curve

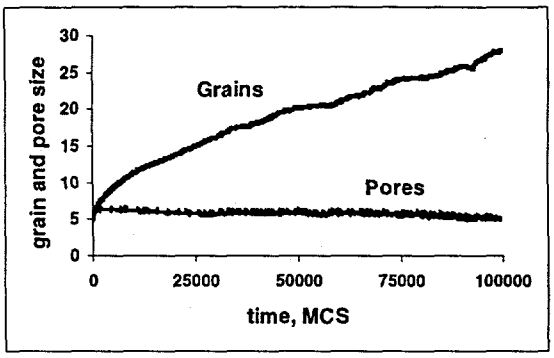

Figure 3. Grain growth and pore growth

3.2 Sintering Stress: The advantage of this MC simulation is that images of microstructural evolution are generated as a function of time during sintering. These simulated microstructures can be used to calculate the interfacial free energy for that microstructure. As a series of microstructures are generated as a function of time, the interfacial free energy as a function of any time dependent variable can also be determine. This information can be used to calculate the sintering pressure and bulk and shear module for continuum scale sintering models. This is a unique ability of this microstructural evolution simulations and to the authors' knowledge has not been done before.

The definition of sintering stress has been reviewed in the previous companion paper [1]. The continuum mechanics definition [37] is

$$P_L \equiv \left.\frac{\partial F}{\partial \vartheta}\right|_T \qquad \text{eq. 3}$$

where F is interfacial free energy and can be obtained by simply measuring the pore surface length of the 2D microstructure shown in figure 1. ϑ is the area of the 2D sintering body and is inversely proportional to the density, $1/\rho$. This, too, is easily obtained from the simulations shown in figure 1. Numerically differentiating the pore surface free energy F with respect to $1/\rho$ gives the sintering stress, which is plotted in figure 4 for the microstructural evolution shown in figure 1. The sintering stress shows a slight increase with increasing density.

Using regression analysis, an analytical approximation of the numerical data is obtained. The analytical approximation used for the normalized effective sintering stress $\overline{P}_L$ is of the form:

$$\overline{P}_L = a(1-\theta)^b \qquad \text{eq. 4}$$

The porosity θ is defined as $1-\frac{\rho}{\rho_T}$, where ρ is density and ρ_T is theoretical densities, respectively. The unknown parameters a and b are determined based on the minimum

square deviations approach. Finally, the following analytical expression for the effective sintering stress is derived:

$$\overline{P}_L = 1.7(1-\theta)^{0.26} \qquad \text{eq. 5}$$

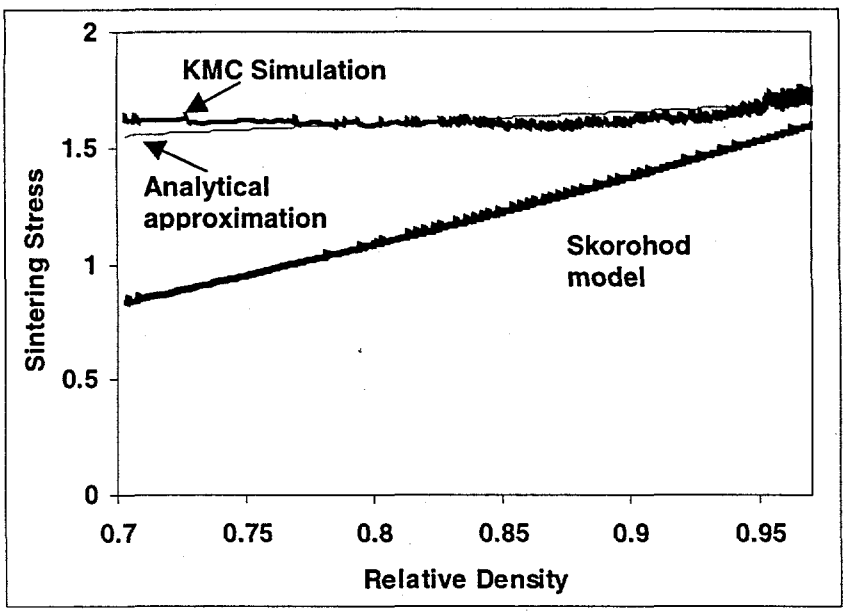

Figure. 4 Comparison of different models for the effective sintering stress

Both numerical and approximate analytical results are plotted in figure 4 and compared to the known expression of Skorohod [38]:

$$\overline{P}_L = (1-\theta)^2 \qquad \text{eq. 6}$$

One can see that like the mesoscale simulations, the values of the effective sintering stress are significantly higher. The difference between two models becomes smaller with higher relative density. This is attributed to the different dimensionality of the two models: the mesoscale simulations are in 2D, whereas, Skorohod's model is based on 3-D (stochastic) analysis.

3.3 Effective normalized bulk modulus. Continuum model of free sintering for a linear-viscous material (see equation 5 of the companion paper [1]), states the first invariants of the stress $\boldsymbol{p}$ and of strain rate $\boldsymbol{e}$ tensors are related as:

$$P_L = -2\eta_o \psi \dot{e} \qquad \text{eq. 7}$$

where η_o is the shear viscosity of the fully-dense substance.; $P_L = P_{Lo}\overline{P}_L$, where P_{Lo} is the local sintering stress. In accordance with the Skorohod's model [38], $P_{Lo} = \dfrac{3\alpha}{r_o}$, where α is the surface tension, r_o is the average particle radius. ψ is the normalized bulk viscosity modulus, which depends on porosity θ, $\dot{e}$ is the first invariant of the strain rate tensor, *i.e.* sum of tensor diagonal components: $\dot{e} = \dot{\varepsilon}_{11} + \dot{\varepsilon}_{22} + \dot{\varepsilon}_{33}$. The condition of continuity can be written as:

$$\frac{\dot{\theta}}{1-\theta} = \dot{e} \qquad \text{eq. 8}$$

The porosity θ is defined as $1-\frac{\rho}{\rho_T}$, where ρ/ρ_T is relative density. Physically, $\dot{e}$ represents the volume change rate of a porous body. From the equations 7 and 8, one can determine the effective normalized bulk modulus ψ:

$$\psi = \frac{-P_L(1-\theta)}{2\eta_o\dot{\theta}}$$

or eq. 9

$$\psi = \frac{-\bar{P}_L(1-\theta)}{2d\theta/d\tau}$$

where τ is the specific time of sintering and is related to real time t as:

$$\tau = \int_0^t \frac{P_{Lo}}{\eta_o} dt \qquad \text{eq. 10}$$

Thus, if the effective sintering stress and the sintering kinetics are known, the modulus ψ can be determined.

In addition to the effective sintering stress, presented in figure 4, the mesoscale simulations enabled the determination of the sintering kinetics (see figure 2). In order to use the mesoscale kinetic information, the KMC simulation time must be related to the one used in the continuum kinetics relationship eq. 9. Time in the KMC simulations is given in unit of Monte Carlo steps, MCS, the number of spin change attempts. As a first approximation, we adjust these two time scales, to calculate the specific time of sintering to match that of the Skorohod model (see eq. 7 above and eq. 15 below), to achieve the same final relative density corresponding to the mesoscale simulations data shown in Fig.2. As a result of equations 7 and 15 below,

$$\tau = \ln\left(\frac{\theta_i}{\theta}\right)^{4/3} \qquad \text{eq. 11}$$

where θ_i is the initial porosity.

This specific time of sintering should be associated with the final number of attempts A_f in conformity to the time scale in Monte-Carlo simulations:

$$\tau \sim A_f \qquad \text{eq. 12}$$

Then, the data in figure 2 can be replotted as a function of specific time of sintering and used to find the specific time derivative of the relative density in eq. 9. As a result, the effective normalized bulk modulus is determined numerically and plotted as a function of porosity in Fig. 5.

Using regression analysis, a relation of the form given by equation 13 is used to fit the numerical data.

$$\psi = \frac{2}{3}\frac{(1-\theta)^c}{\theta^d} \qquad \text{eq. 13}$$

The unknown parameters c and d are determined based on the minimum square deviations approach. Finally, the following analytical expression for the effective normalized bulk modulus is derived:

$$\psi = \frac{2}{3}\frac{(1-\theta)^{2.23}}{\theta^{1.12}} \qquad \text{eq. 14}$$

Both numerical and approximate analytical results are plotted in Fig. 5 and compared to the known expression of Skorohod [38]:

$$\psi = \frac{2}{3}\frac{(1-\theta)^3}{\theta} \qquad \text{eq. 15}$$

One can see that, in accord with the mesoscale simulations, the values of the effective normalized bulk modulus are lower. The difference between two models becomes smaller with higher relative density. Similar to the deviations in the effective sintering stress, this should be attributed to the different dimensionality of the two models: the mesoscale simulations assume a 2-D unit cell, and Skorohod model is based on 3-D (stochastic) analysis.

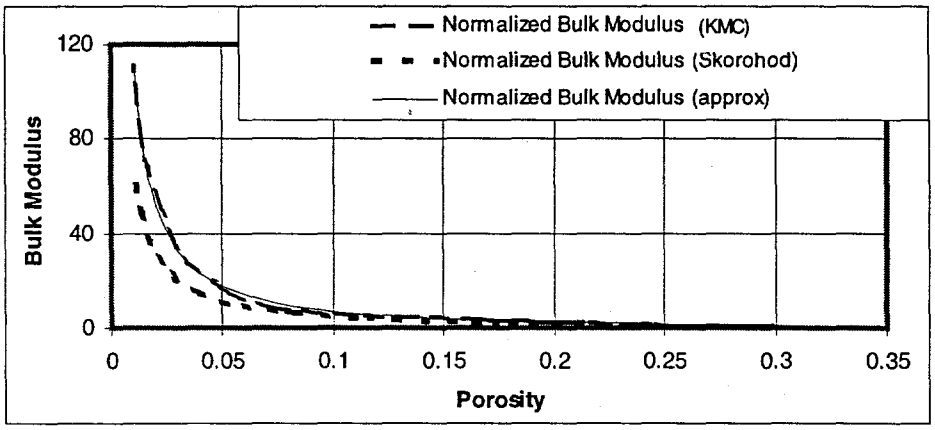

Fig. 5 Dependence of the normalized effective bulk modulus on porosity

Using the determined analytical expressions eq. 5and eq. 15 for the effective sintering stress and the effective normalized bulk modulus, and solving eq. 7, one can determine the sintering kinetics (the time dependence of relative density or porosity).

4. Discussion

The simulation of microstructural evolution on the mesoscale is important and interesting for understanding many aspects of sintering. It is useful to study the effect of particle size and shape, the transport mechanisms, interfacial energies and others properties on sintering and the resulting microstructures. However, as shown in this work, the utility of mesoscale simulations for sintering goes beyond this. Mesoscale simulations can be used to generate the materials parameters necessary for accurate simulation of sintering of the macroscopic, continuum scale to predict dimensional changes in a sintering body. Furthermore, control of these materials parameters (sintering stress, bulk modulus, etc) during sintering may be possible by manipulation of microstructural evolution. This possibility makes a combination of these mesoscale and continuum models a powerful set of tools for use in predicting and controlling dimensional changes during sintering.

The model and results presented here are all for sintering in two dimensions, while real materials are three dimensional. While results of many problems of microstructural evolution in 2D are readily extendable to 3D, sintering of porous single materials is probably not. In the 2D simulations presented here, the porosity is isolated and not percolating even at 30% as seen in figure 1. This is not the case in 3D, where porosity is continuous and interconnected for porosity greater than ~8% depending on the specifics of that system [7,14,16]. Below ~8% porosity, the pore become isolated. These topological differences in 2D and 3D are expected to give some fundamental difference in microstructural evolution for the two cases. Future research will address the MC simulation of sintering in 3D.

5. Conclusions

In addition to studying microstructural evolution during sintering, kinetic Monte Carlo simulations can be used to generate material parameters, such as sintering stress and bulk modulus necessary for accurate simulation of shrinkage and deformation of macroscopic sintering parts.

Acknowledgement: Sandia is a multiprogram laboratory operated by Sandia Corporation, a Lockheed Martin Company, for the United States Department of Energy under the Contract DE-AC04-94AL-85000.

---

[1] E.A. Olevsky and V. Tikare, "Combined Macro-Meso Scale Modeling of Sintering. Part I: Continuum Approach, *this publication.*
[2] G.C. Kuczynski, "Self-Diffusion in Sintering of Metal Particles", *Trans. Amer. Inst. Min.*, 185 169-178 (1949).
[3] W.D. Kingery and M. Berg, *J. Appl. Phys.* 26 1205-? (1955)
[4] H.E. Exner, Acta Metall. 35 587 (1987). H.E. Exner, "Principles of Single Phase Sintering," *Rev. Powder Metall. Phys. Ceram.*, 1 7 (1979).
[5] D.L. Johnson and I.B. Cutler, *J. Amer. Ceram. Soc.* 46 541(1963); D.L. Johnson and T.M. Clarke, *Acta Metal.*, 12 1173 (1964); D.L. Johnson, *J. Appl. Phys.*, 40 192 (1969).
[6] R.L. Coble, *J. Amer. Ceram. Soc.* 41 55 (1958)
[7] F.B Swinkels and M.F. Ashby, *Acta Metall.*, 29, 259 (1983).
[8] F.A. Nichols and W.W. Mullins, *J. Applied Phys.* 36 1826 (1965).
[9] N. Cabrera, *Trans. AIME.*, 188, 667 (1950).
[10] R.M. German and J.F. Lathrop, *J. Mater. Sci.*, 13 921 (1978).
[11] R.T. DeHoff in Science of Sintering: new directions for materials processing and microstructural control, edited by D.P. Uskokovic *et al.* Plenum Press, New York (1989)
[12] D. Bouvard and R.M. McMeeking, *J. Am. Ceram. Soc.*, 79 [3] 666 (1996).
[13] J. Svoboda, H. Riedel H. Zipse, *Acta Metall.*, 42 [2] 435 (1994)
[14] H. Riedel, H. Zipse and J. Svoboda, *Acta Metall.* 42 [2] 445 (1994).
[15] M.A. Occhionero, J.W. Halloran in Sintering and Heterogeneous Catalysis edited by G.C. Kuczynski, Albert E. Miller, Gordon A. Sargent, Plenum Press, New York (1984)
[16] J. Zhao, M.P. Harmer, *J. Am. Ceram. Soc.*, 71 [2] 113 (1988); J. Zhao, M.P. Harmer, *J. Am. Ceram. Soc.*, 71 [7] 530 (1988).
[17] T. Ikegami, *Acta Metall.*, 35 667 (1987).
[18] P.Zeng, S. Zajac, P.C. Clapp and J.A. Rifkin, *Mat .Sci. & Eng.*, A252 301 (1998).
[19] K. Tsuruta, A Omeltchenko, R. K. Kalia, and P. Vashishta, *Mater. Res. Soc. Symp. Proc.* vol. 408 (1996): K. Tsuruta, A Omeltchenko, R. K. Kalia, and P. Vashishta, *Euro. Phys. Lett.* 33, 441 (1996).
[20] Zhang & Scheibel, *Acta Metall*, 43, 4377 (1995).
[21] Zhou & Derby, *J. Am. Ceram. Soc.*, 81, 478 (1998).
[22] Jagota & Dawson, *Acta Metall.*, 36, 2551 (1988).
[23] Pan et al., *Acta Metall.*, 13, 4671 (1998)
[24] J.W. Bullard, *J. Appl. Phys.* 81 [1] 159-168 (1997).
[25] G.N. Hassold, I-W, Chen. D.J. Srolovitz, *J. Am. Ceram. Soc.*, 73 [10]2857-64 (1990); I-W. Chen, G.N. Hassold and D.J. Srolovitz, *J. Am. Ceram. Soc.*, 73 [10] 2865 (1990).
[26] M.P. Anderson, D.J. Srolovitz, G.S. Grest, and P.S. Sahni, *Acta Metall.* 32 [5] 783-791 (1984).
[27] J. Wejchert, D. Weaire, J.P. Kermode, *Phil. Mag. B*53 15-24 (1986).
[28] E.A. Holm, James A. Glazier, D.J. Srolovitz, G.S. Grest, *Phys. Rev. A*, 43 [6] 2662-2668 (1991).
[29] D.J. Srolovitz, G.S. Grest, M.P. Anderson, and A.D. Rollett, Acta Metall., 36 [8] 2115-2128 (1988).
[30] V. Tikare and J.D. Cawley, *Acta Metall.*, 46[4] 1343-1356 (1998).
[31] V. Tikare and E.A. Holm, *J. Am. Ceram. Soc.*, 81[3] 480-484 (1998).
[32] F. Y. Wu, *Rev. Modern Phys.*, 54 [1] 235-268 (1982).
[33] V. Tikare and E.A. Holm, *J. Am. Ceram. Soc.*, 81[3] 480-484 (1998).
[34] V. Tikare and J. Cawley, *J. Am. Ceram. Soc.*, 81 [3] 485-91 (1998).
[35] B.H. Alexander and R.W. Balluffi, *Acta Metall.* 5 666677 (1957).
[36] V. Tikare, M.V. Braginsky, E.A. Olevsky, R.T. DeHoff accepted for publication in Sintering '99 edited by R.M. Randall and G. Messing.

[37] E.A. Olevsky, *Mat. Sci. & Eng.*, *R*23 [2] 41 (1998)
[38] V.V. Skorohod, Rheological Basis of the Theory of Sintering, Kiev, Naukova Dumka (1972)